

# The Fermi Bubbles Revisited

Rui-zhi Yang<sup>1,2</sup>, Felix Aharonian<sup>1,3</sup>, and Roland Crocker<sup>4,1</sup>

<sup>1</sup> Max-Planck-Institut für Kernphysik, P.O. Box 103980, 69029 Heidelberg, Germany

<sup>2</sup> Key Laboratory of Dark Matter and Space Astronomy, Purple Mountain Observatory, Chinese Academy of Sciences, Nanjing, 210008, China

<sup>3</sup> Dublin Institute for Advanced Studies, 31 Fitzwilliam Place, Dublin 2, Ireland

<sup>4</sup> Research School of Astronomy and Astrophysics, Australian National University, Canberra, Australia

Preprint online version: July 13, 2021

## ABSTRACT

We analyze 60 months of all sky data from the *Fermi*-LAT. The Fermi Bubble structures discovered previously are clearly revealed by our analysis. With more data and, consequently, better statistics we can now divide each bubble into constant longitude slices to investigate their gross  $\gamma$ -ray spectral morphology. While the detailed spectral behaviour of each slice derived within our analysis is somewhat dependent on the assumed background model, we find, robustly, a relative deficit of the flux at low energies (i.e., hardening) towards the top of the South Bubble. In neither Bubble does the spectrum soften with longitude. The morphology of the Fermi Bubbles is also revealed to be energy dependent: at high energies they are more extended. We conclude from the gamma-ray spectrum at high latitudes that a low energy break in the parent cosmic ray population is required in both leptonic and hadronic models. We briefly discuss possible leptonic and hadronic interpretation of this phenomenology.

**Key words.** Gamma rays: diffuse background, ISM: cosmic rays

## 1. Introduction

Two huge, bubble-like structures have been reported by Su et al. (2010), Dobler et al. (2010), and Su & Finkbeiner (2012) in *Fermi*-LAT gamma ray data to extend  $\sim 50^\circ$  above and below the Galactic center. The gamma ray emission from these structures, dubbed the ‘Fermi Bubbles’ (FBs), exhibits a  $E^{-2}$  type spectrum, significantly harder than the spectrum of the diffuse gamma-ray emission from the Galactic disk. Remarkably, structures coincident or similar to the FBs can be seen at other wavelengths, including the (total intensity) microwave haze found in WMAP (Finkbeiner 2004) and, most recently, in Planck data (Planck Collaboration et al. 2013); the polarized microwave structures reported by Jones et al. (2012); the large-scale, biconical structures found (Bland-Hawthorn & Cohen 2003) in ROSAT X-ray data (Snowden et al. 1997); and the giant polarised radio lobes recently found at 2.3 GHz (Carretti et al. 2013). Several models have been proposed to explain both the morphology and spectral properties of the FBs (Cheng et al. 2011; Mertsch & Sarkar 2011; Crocker & Aharonian 2011; Crocker 2012; Zubovas et al. 2011; Zubovas & Nayakshin 2012; Guo & Mathews 2012; Guo et al. 2012; Yang et al. 2012; Crocker et al. 2013). These models predict different energy dependent morphologies. For example, in the simplest IC model (e.g., discussed by Su et al. 2010) with a spatially-independent electron spectrum described by a power law electron population with a low energy cutoff at 500 GeV, one expects a tendency for softening of the gamma-ray spectra at high latitudes. This is due to the gradual reduction of the IC components produced via upscattering of the optical and UV photons - the main target fields contributing to the production of gamma-rays above 10 GeV that also decline towards high latitudes. On the other hand, in a simple one-zone hadronic model (e.g., Crocker & Aharonian 2011) the protons’ steady state distribution should produce a similar spectrum of gamma rays at all latitudes. Thus, studies of the energy-dependent morphology of the FBs may shed light on the nature of the gamma ray emission mechanism(s). This is the basic motivation for the current study.

Here we present an analysis based on 60 months’ *Fermi*-LAT data. We find a similar overall morphology and spectrum for the FBs to those obtained by Su et al. (2010). The FBs exhibit a rather homogeneous *surface* brightness. Importantly, this implies non-homogeneous *volumetric* emissivities considering projection effects (Su et al. 2010). The FBs, however, are not completely uniform: they exhibit some ‘hot spots’ (referred to by Su et al. (2010); Su & Finkbeiner (2012) as the ‘jet’, ‘donut’ and ‘cocoon’).

In this paper the significantly larger photon statistics and the availability of the recently updated Fermi science software tools (Ackermann et al. 2012) allow us to investigate the gross spectral morphology of the FBs. A somewhat similar study has recently been conducted by Hooper & Slatyer (2013). However, they concentrate spectral features in low latitudes while we focus on the high latitude, especially the top of the bubble. We proceed by dividing each bubble into several slices to investigate possible gamma-ray spectral change with latitude. Employing different background models, we find, robustly, a spectral hardening, or more specifically, a deficit of low energy flux towards the top of the SFB. We are also able to extend the spectrum of the FBs to lower energy than previously attempted because of the improvement of the analysis software and the instruments response functions. The paper is structured as follows: in section 2 we present

52 the results of our data analysis, in section 3 we discuss the fitting of leptonic and hadronic models to the gamma ray  
 53 data, and in section 4 we set out our conclusions.

## 54 2. Data Analysis

55 We use the publicly-available data obtained by the *Fermi*-LAT in the gamma-ray energy interval from 100 MeV to 300  
 56 GeV over the period of 4 Aug 2008 and 17 July 2013 (MET 239557417 - MET 395797613). To avoid contamination from  
 57 charged particles we use the *ULTRACLEAN* data set in the analysis. We adopt the instrument response function version  
 58 P7V6 (Ackermann et al. 2012). All events are binned in the all-sky map in HEALPIX format with *NSIDE*=256. The  
 59 sources in the 2<sup>nd</sup> Fermi catalog (Abdo et al. 2012) are subtracted from the counts map using the flux in the catalog.  
 60 To take into account the energy dependent point spread function (PSF) of the *Fermi*-LAT, we use the functional form  
 61 described in the LAT homepage<sup>1</sup> when masking sources in the catalog.

62  
 63 We use a likelihood method for determining the FBs' apparent morphology and spectral features for different diffuse  
 64 emission templates. The likelihood function has the form  $\log(L) = \sum_{k_i} \log(\mu_i) - \mu_i - \log(k_i!)$ , where  $k$  is the number  
 65 of photons in the  $i$ -th bin in the counts map and  $\mu_i$  is the predicted number of photons within a particular linear  
 66 combination of the templates. The sum is over all the spatial bins in the map. The likelihood function is determined in  
 67 different energy bins to derive the energy spectrum. For fitting different energy bins, rather than smoothing the map  
 68 to an universal FWHM (full width at half maximum) as used in Su et al. (2010), we only smooth the diffuse templates  
 69 with the Fermi PSF and then fit the counts map as a linear combination of these smoothed diffuse templates. The  
 70 normalization of each diffuse template is left free in the likelihood fitting. We do not assume *a priori* the existence of a  
 71 pair of bubble-like structures. We only use the spatial templates for  $\pi^0$  decay and IC gamma-rays generated by GALPROP  
 72 (Vladimirov et al. 2011) in addition to the isotropic template related to the extragalactic gamma ray background and  
 73 cosmic ray contamination. Finally, we take into account the large diffuse structure high above the plane to Galactic north  
 74 which may be connected with the nearby ISM feature Loop 1 (Su et al. 2010). In generating the diffuse templates with  
 75 GALPROP, we adopt the default Galdef webrun setting, the 2D plane diffusion model that was tuned to fit the ACE  
 76 data.

77 After subtracting the best-fit linear combination of the diffuse templates, we find residual maps. By summing over  
 78 all energy bins above 1 GeV we obtain the image in Fig. 1 in which two bubble-like structures are clearly seen. Next we  
 79 generate spatial templates for the FBs from the residual map. In the second step of our analysis these Bubble templates  
 80 are included. We employ the likelihood method mentioned above once again and obtain the spectrum of all the diffuse  
 81 templates.

82 To derive the spectrum in different parts of the FBs, we divide the SFB ( $-55^\circ < b < -25^\circ$ ) into four slices and the  
 83 North Fermi Bubble ( $25^\circ < b < 50^\circ$ ; 'NFB') into three. To avoid contamination from the Galactic plane, in the fitting  
 84 we mask out the inner  $\pm 25^\circ$  region. The position of each analysis slice can be found in Fig. 3. The SED of each slice  
 85 is shown in Fig. 2 where the numbers 1 to 4 run from lowest to highest latitude. From the SEDs it is evident that the  
 86 spectrum of the highest southern slice is in deficit at low energies relative to the other slices. It is important to note that  
 87 this same slice suffers little from geometric projection effects and is thus a true reflection of the spectrum at the top of  
 88 the SFB. The spectrum at the top of the SFB is, therefore, significantly different from that in the interior. Fig. 3 reveals  
 89 the different morphologies of the FBs in different energy bins; at high energies the SFB is clearly more extended than at  
 90 low energies. This is highlighted in Fig. 4. It should also be noted that in the top slice of the SFB (South 4) there are no  
 91 known point sources from the 2<sup>nd</sup> Fermi catalog, making our conclusion about the spectral variation quite robust.

92 Regarding the energy-dependent morphology of the FBs, we also flag the following point to be dealt with in further  
 93 work: as evident from figs. 3 and 4, the SFB is also relatively more extended to Galactic *west* at high energies than low  
 94 energies implying a spectral hardening going from east to west. As far as we are aware, no model for the FBs currently  
 95 accounts for this effect. It is interesting that, because of this extension to the west, at high energies, the FBs come to  
 96 more closely resemble the polarised radio lobes detected at 2.3 GHz (Carretti et al. 2013)<sup>2</sup>.

97 Accurate determination of the morphology and spectral features of the Bubbles strongly depends on reliable modeling  
 98 of the diffuse background. Unfortunately, because of uncertainties in the distributions of cosmic rays and interstellar  
 99 gas, our knowledge about the diffuse gamma-ray background is imperfect. In such circumstances, one can only introduce  
 100 different *templates* that instantiate different estimates of the background and try to derive the true Bubble flux with them  
 101 using a likelihood method. Unfortunately, different choices of background templates alter the final result significantly  
 102 and this may lead to significant systematic errors. To study such possible errors, we investigate the 128 GALPROP  
 103 models listed by Ackermann et al. (2012). The aim of Ackermann et al. (2012) was to study the origin and propagation  
 104 of cosmic-rays and the distribution of the interstellar medium by simultaneously fitting diffuse gamma ray emission and  
 105 cosmic ray data. Although all their models underestimate the GeV emission at low latitudes (Ackermann et al. 2012),  
 106 this has little influence on our results given our masking of the inner  $\pm 25^\circ$  when deriving spectra. The 128 models  
 107 are different in cosmic ray (CR) source distribution, CR halo size, HI spin temperature and  $E(B - V)$  magnitude cut.  
 108 Following perusal of the the online material for Ackermann et al. (2012), we found that 64 models with  $z = 8$  kpc and  
 109  $z = 10$  kpc do not fit the  ${}^9\text{Be}/{}^{10}\text{Be}$  data well (the derived curves fall outside of the error bars of nearly all the data

<sup>1</sup> [http://fermi.gsfc.nasa.gov/ssc/data/analysis/documentation/Cicerone/Cicerone\\_LAT\\_IRFs/IRF\\_PSF.html](http://fermi.gsfc.nasa.gov/ssc/data/analysis/documentation/Cicerone/Cicerone_LAT_IRFs/IRF_PSF.html)

<sup>2</sup> RMC thanks Ettore Carretti for raising this point in conversation.

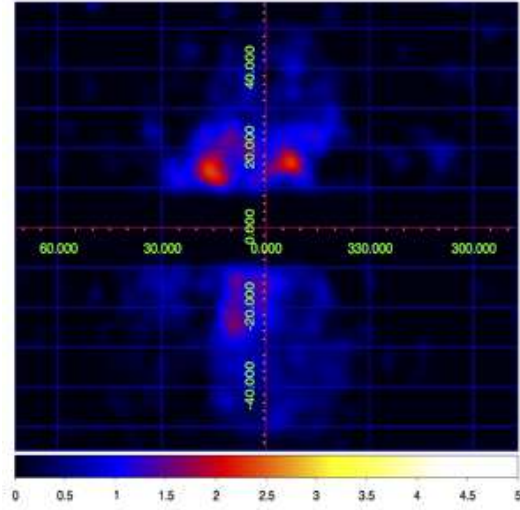


**Fig. 1.** The residual map above 2 GeV. Background subtraction is described in the text. Two bubble-like structures can be seen. To render the picture clearer we mask the bright Galactic plane  $|b| < 5^\circ$

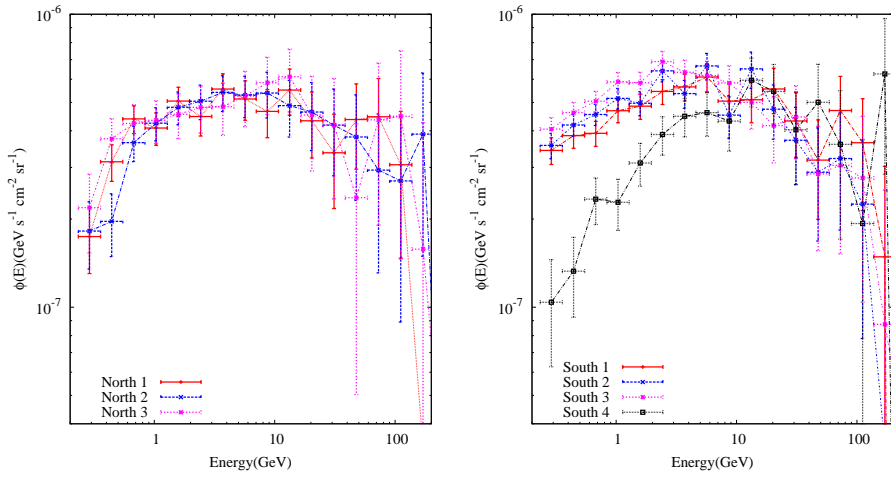


**Fig. 2.** SEDs of different slices of the North and South FBs. The numbers 1 to 4 run from low to high latitudes. Left panel: North Bubble (NFB), Right panel: south Bubble (SFB).

110 points), where  $z$  is the height of the CR halo. Therefore we abandon these, and investigate the other 64 models as diffuse  
 111 emission templates.

112 With the same procedure as described above, we find the SEDs in different slices with all chosen templates; the results  
 113 are summarized in Fig. 5. Because of the large systematic errors, we may not claim a deficit at low energies and high  
 114 latitude in the NFB. However, in the SFB the low energy deficit of the top slice is significant for every template. It should  
 115 be noted that, due to the slight differences in overall flux normalisation for the different templates choices, differences of  
 116 spectral shape are smeared out if we plot them all together as in Fig. 5 which, therefore, suggests a smaller difference  
 117 between the top and bottom slices than exists in reality. In Fig. 6 we show 8 examples of SEDs for the slices in the SFB  
 118 which give the extreme cases of the gamma ray flux. From these individual examples the low energy deficit in the top  
 119 slice is much more evident. Results for the northern slices are also shown in Fig. 7 which reveal the low energy part of  
 120 the top slice has very large uncertainties. The large systematics in the NFB are likely due to the fact that it is partially  
 121 coincident with the extended Loop 1 structure whose physical origin and exact morphology and spectral features are still  
 122 uncertain.

### 123 3. Discussion

124 The gamma-ray residual maps obtained in the current study – based on six years’ *Fermi*-LAT data – confirm that the  
 125 surface brightness of each bubble is homogeneous at a gross level. This implies that the *volumetric* emissivity is not  
 126 homogeneous, otherwise we would detect a higher brightness in the center of each bubble due to projection (Su et al.  
 127 2010). One possible explanation of this may be higher turbulence in the bubbles’ edges generating more efficient particle  
 128 acceleration or stronger confinement of high energy particles there with a resulting increase in the local gamma ray

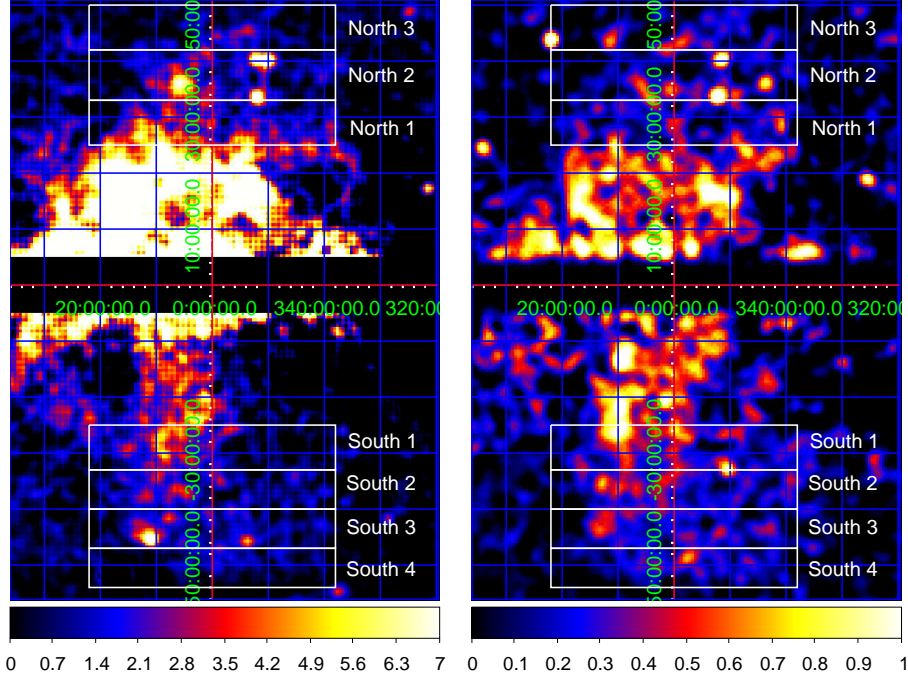


**Fig. 3.** Residual maps for different energy bins. The left and right panels correspond to energy intervals 1 – 2 GeV and 10 – 30 GeV, respectively. The inner disk of the Galaxy ( $|b| < 2^\circ$ ) is masked. The boxes laid over the residual maps show the position of each slice.

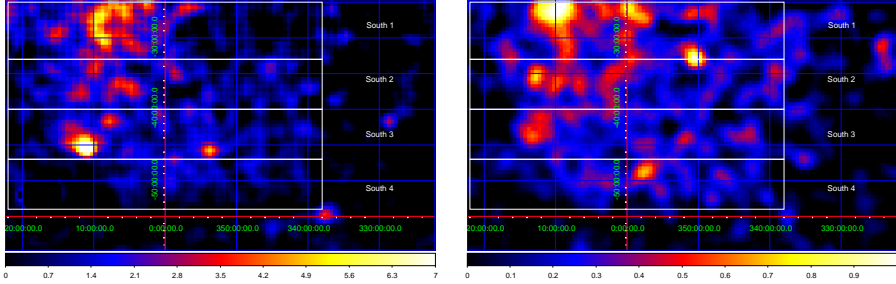


**Fig. 4.** Zoom in of Fig. 3 for the SFB region. Left panel 1 – 2 GeV and right panel 10 – 30 GeV.

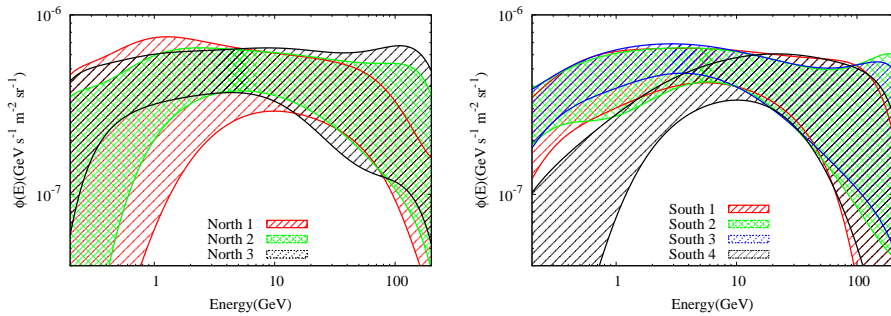


**Fig. 5.** The SEDs for the seven slices with all 64 templates we use in our analysis. The shaded areas span all derived SEDs. The left panel is for the NFB while the right is for the SFB.

129 emissivity; alternatively, in a non-saturation hadronic model, higher gas densities towards the edges may have the same  
 130 effect (Crocker et al. 2013).

131 Below we assume the low energy deficit of the gamma ray spectrum at high latitudes found above is a real effect and  
 132 discuss its possible implications.

133

134 To simplify our modeling, we assume each bubble is a sphere with a radius 3.4 kpc. The 2-d projection of each  
 135 bubble can be approximated as a half sphere in the region  $b > 30^\circ$  for the NFB and  $b < -30^\circ$  for the SFB. The

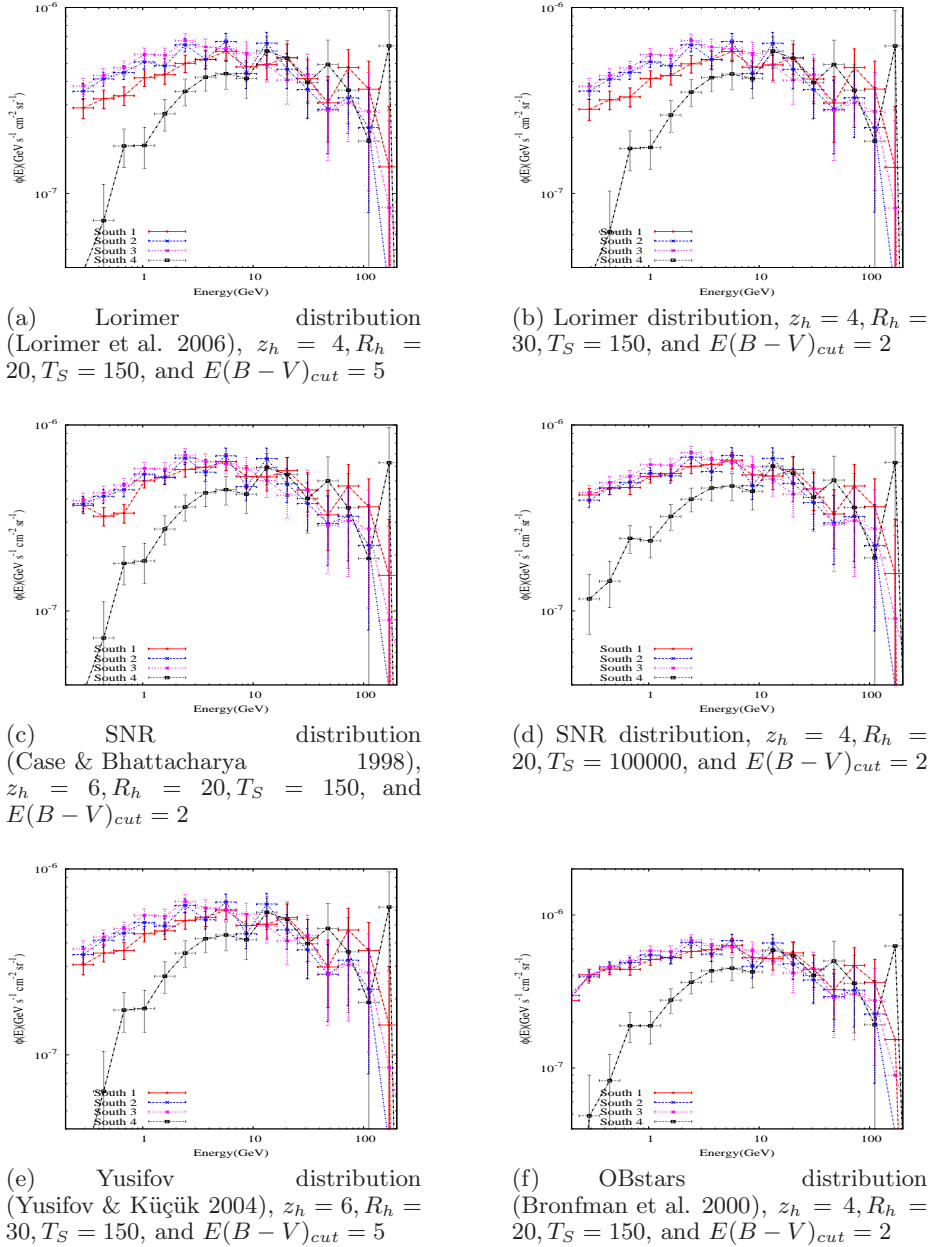


**Fig. 6.** Six examples of SEDs for slices in the SFB.

136 center of each bubble is located at  $(0,0,\pm 5\text{kpc})$  in Galactic coordinates. Assuming an *intrinsic* north-south symmetry,  
 137 we only analyse the SFB and, to reveal most starkly the spectral change with latitude, we consider only slice South 1  
 138  $(-33^\circ < b < -25^\circ)$  and South 4  $(-55^\circ < b < -47^\circ)$  in detail. Slice South 1 covers the center of the SFB. We use the  
 139 ISRF value in Galprop at  $(0,0,5\text{ kpc})$  for the average value of the slice South 1 in the calculation,  $w_{IR} = 0.18\text{ eV/cm}^3$   
 140 and  $w_{opt} = 0.9\text{ eV/cm}^3$ . The height of South 4 is about 7 kpc, thus we adopt the ISRF energy density from Galprop  
 141 at  $(0,0,7\text{ kpc})$ ,  $0.7\text{ eV/cm}^3$  for the optical component and  $0.15\text{ eV/cm}^3$  for the IR component. The IR and optical  
 142 photon fields are modeled as diluted blackbody (gray body) spectra with temperatures of 100 K and 5000 K, respectively.  
 143

144 In the hadronic scenario, motivated by the relative low energy deficit of the gamma ray flux in the top slice, we fit the  
 145 SED in South 1 with a pure power law proton spectrum while for South 4 we use a power law with a low energy break  
 146 that we find needs to be at 20 GeV to fit the data. We assume the proton flux below the break is zero for simplicity (see  
 147 Fig. 8). Our results are shown in Fig. 9. The required low energy break may arise naturally due to energy-dependent  
 148 diffusion effects in a non-steady-state scenario: given South 4 is far from the (assumed) injection source in the plane,  
 149 it may be that only high energy particles (which diffuse faster) have had time to travel there since a previous injection  
 150 event or given the age of the structure. The formalism describing these energy-dependent diffusion effects can be found in  
 151 Aharonian & Atoyan (1996) where both impulsive and continuous injection cases are described. The position of the low  
 152 energy break can be estimated by equating the age of the bubble (or the time since a previous burst) with the diffusion

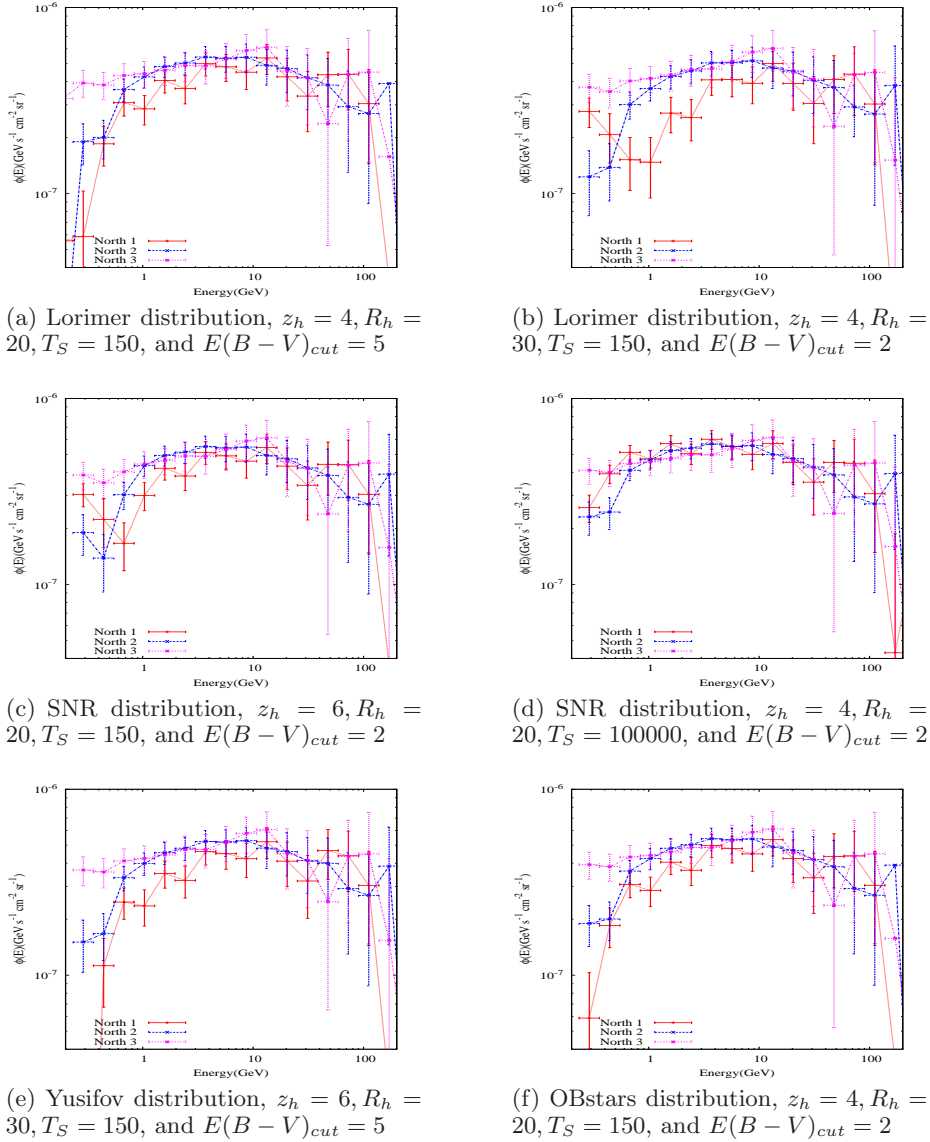


**Fig. 7.** Six examples of SEDs for slices in the NFB.

153 time, i.e., the beak energy is  $E_{bk} \simeq (d^2/(D_0 t))^{1/2}$ , where  $d$  is the distance of the top slice from the injection source,  $t$  is  
 154 the age of the bubble (or burst) and  $D(E) = D_0 E^\delta$  is the energy dependent diffusion coefficient. If we assume protons  
 155 are injected at the Galactic center,  $d$  is about 7 kpc. Notice that in the kinetic equations which govern proton diffusion  
 156 only the combination  $D_0 t$  appears. Thus any timescale can be obtained if we tune the diffusion coefficient  $D_0$ . If  $D(E)$   
 157 takes a value similar to that in the Galactic plane, say  $4 \times 10^{28} \text{ cm}^2 \text{ s}^{-1}$  at 1 GeV and  $\delta = 0.3$ , the age of the FBs should  
 158 be  $t \sim 10^8 \text{ yr}$  (cf. Crocker et al. 2013). Alternatively, if there is continuous proton injection into the FBs over  $10^{10} \text{ yrs}$   
 159 we need a rather small diffusion coefficient,  $D_0 \sim 10^{26} \text{ cm}^2 \text{ s}^{-1}$  at 1 GeV, which is about 1/100 of that in the Galactic  
 160 plane.

161 If we assume the injection is impulsive and the ISM density is  $0.005 \text{ cm}^{-3}$  the total energy in protons needed to light  
 162 the Bubbles is of the order  $10^{56} \text{ erg}$ . Note that if we assume the simple geometry mentioned above and a magnetic field  
 163  $B \sim 10 \mu\text{G}$  as suggested by Carretti et al. (2013), then the energy densities of cosmic rays and magnetic fields are close  
 164 to equipartition. A burst-like injection event requires that the duration of the injection is much smaller than the age of  
 165 the structure which is  $t \sim 10^8 \text{ yr}$  (for  $D_0 = 4 \times 10^{28} \text{ cm}^2 \text{ s}^{-1}$  at 1 GeV), i.e., the duration of the injection event would  
 166 have to be of order  $10^7 \text{ yr}$  or less in this case. Then the injection rate is of the order  $10^{41} \text{ erg/s}$ , two orders of magnitude  
 167 larger than the the X-ray luminosity of a X-ray reflection nebulae near the Galactic center (e.g., Gando Ryu et al. 2012),  
 168 but still only one thousandth of the Eddington Luminosity of Sgr A\*,  $\sim 5 \times 10^{44} \text{ erg/s}$ .

169 A possible concern for an energy-dependent diffusion scenario is that, in the high energy range for which the diffusion  
 170 length is much larger than the distance to the source, the predicted proton density should be the same at all latitudes  
 171 for the impulsive case, or scale as  $1/R$  (where  $R$  is the distance to the injection source) for the continuous case. Thus,  
 172 given the (expected) relatively smaller line of sight through the top of the SFB, one naively anticipates that the gamma  
 173 ray flux in South 4 is smaller than that in South 1. The observed data reveal a similar total flux in both slices at high

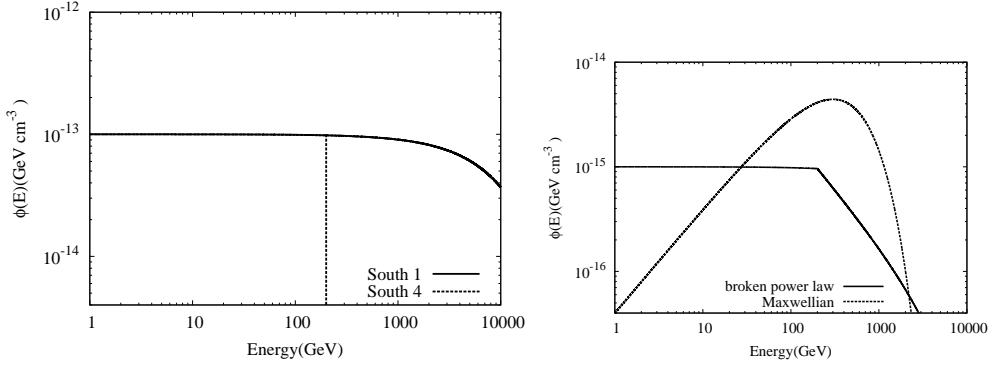


**Fig. 8.** Assumed CR proton (left) and electron (right) distributions in Slices 1 and 4 of the SFB

174 energy, however. One possible resolution to this tension may be that the target gas density is higher at high latitudes.  
 175 It is also likely that the geometry of the FBs is different from our simple assumption of sphericity thereby entailing  
 176 non-trivial projection effects.

177

178 In a leptonic scenario the low energy deficit of gamma ray flux in the top slice also requires a corresponding low  
 179 energy break in the electron distribution (see Fig. 8 right). This can, again, be produced by several mechanisms. Firstly,  
 180 the energy-dependent diffusion effects mentioned above also work for electrons in principle (cf. McQuinn & Zaldarriaga  
 181 2011). However the much faster cooling of electrons relative to protons tends to prevent such effects playing an important  
 182 role. To fit the high energy gamma ray data we need TeV electrons, whose cooling time scale is about  $10^5$  yrs in the  
 183 circumstances of the FBs. Thus, even if we assume very fast diffusion with the diffusion coefficient of  $4 \times 10^{29}$  cm<sup>2</sup>/s at  
 184 1 GeV (and an index of 0.6), the diffusion distance of TeV electrons in  $10^5$  yrs is only 2 kpc, significantly less than the  
 185 distance of South 4 from the plane (which is more than 5 kpc). This implies high energy electrons accelerated at low  
 186 latitudes can never reach South 4 and, as a result, if we want to explain the radiation of the FBs in a leptonic scenario,  
 187 the electrons should be accelerated *in situ*.

188

189 The second problem related to electrons concerns the interpretation of the very hard energy spectrum of radiation  
 190 below 5 GeV. Such a hard spectrum formally can be explained by assuming a low energy break in the electron spectrum.  
 191 However, if the electrons are cooled, no matter how hard the injection spectrum is, because of the radiative ( $dE/dt \sim E^2$   
 192 type) losses the resulted *steady-state* distribution below the break in the injection spectrum, will have a standard,  
 193  $E^{-2}$  power law-spectrum. The latter will result in IC gamma-ray spectrum with a photon index 1.5 which is still not  
 194 sufficient to explain the observed gamma-ray spectrum of South 4; below 5 GeV the photon index of the latter is as small  
 195 as 1. One can formally overcome this problem assuming that the electrons stay uncooled in FBs. However in order to  
 196 reproduce the break in the gamma-ray spectrum, one would need a corresponding break at 100 GeV. The corresponding  
 197 synchrotron cooling time at this energy,  $t \sim 8 \times 10^5 (\frac{100 \text{ GeV}}{E}) (\frac{B}{10 \mu\text{G}})^{-2}$  yr, appears significantly shorter than the age  
 198 of FBs within any reasonable model of the latter. Thus we need very efficient continuous acceleration of  
 199 electrons which would dominate over the rate of energy losses and in that way keep very hard the steady-state spectrum.  
 200 This in principle can be realized with stochastic acceleration which can produce Maxwellian type *steady-state* energy  
 201 distribution of electrons. Indeed adopting an electron distribution like  $N(E) \sim E^2 \exp(-E/E_0)$  with  $E_0 = 300$  GeV,  
 202 we can have a reasonable fit to the detected gamma-ray spectrum in South 4, as it is shown in Fig. 9. For comparison,  
 203 we also show IC emission at the position of South 1 and South 4 by adopting a broken power law electron distribution  
 204 with an index 2 below the break at 200 GeV and 3 above. The results fit the SED of South 1 well, but fail to fit that of  
 205 South 4, which are also shown in Fig. 9.

206 Anisotropy effects may, in principle, increase the IC gamma ray flux at high latitudes since most of seed photons  
 207 come from regions in the Galactic plane; thus gamma-rays we detect at high latitudes are a result of (almost) head-on  
 208 collisions. To probe this effect we use the formalism described in Moskalenko & Strong (2000). The enhancement factor  
 209 is defined by the flux ratio of the anisotropic IC to the isotropic IC assuming the the same ISRF energy density. Results  
 210 for the positions of South 1 and South 4 are shown in Fig. 9. We can see that although the anisotropic IC effect may  
 211 cause a spectral a hardening, however the difference between South 1 and South 4 is rather small, less than 10%. It  
 212 appears not sufficient to explain the very hard spectrum of South 4.

## 213 4. Summary

214 In this paper we re-analyze the *Fermi*-LAT data covering the FB region. With an improved instrumental response  
 215 function and more data, we are able to extend the previously obtained spectrum to lower energies. Furthermore we  
 216 divide each bubble into slices to investigate possible variation of the spectrum with latitude. Given the improved data,  
 217 for the first time, we can determined robustly that the spectrum of the top of South Bubble drops appreciably at low

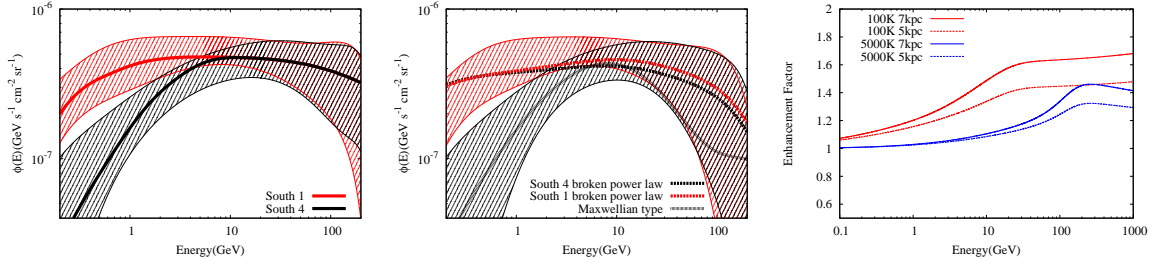


**Fig. 9.** Left and Middle panel: Fitting the FBs' SED with the hadronic model (left panel) and the leptonic model (middle panel) described in the text. The red curve shows the fitted spectrum and the red hatched region spans all spectra resulting with from different templates for South 1; blue curve and hatched region are for South 4. For leptonic models, for South 1 we assume the broken power law described in the text and the ISRF value given by GALPROP. For South 4, the black curve is for the same broken power law with the ISRF floating while for the gray curve we use the ISRF in GALPROP at the position of South 4 and a Maxwellian type electron distribution with  $E_{bk} = 300$  GeV. In our hadronic scenario energy dependent diffusion effects are considered as described in the text. Right panel: The enhancement factor due to anisotropic IC. The IR and Opt/UV components of the ISRF have effective temperatures of 100 K and 5000 K, respectively. Results for  $z = 5$  kpc and  $z = 7$  kpc are shown (approximate heights of South 1 and South 4 above the Galactic plane).

218 energies relative to the spectrum determined at lower latitudes. We also show that the morphology of the South Bubble  
 219 is energy dependent; at high energy the structure is relatively more extended to both Galactic south and west.

220 We have also investigated the influence of different choices of background model on the results of our analysis. We  
 221 found that background models may significantly alter the apparent gamma-ray signal from the FBs. Nevertheless, the  
 222 spectral hardening with latitude in the South Bubble remains a robust result. In neither Bubble do we find a spectral  
 223 *steepening* with latitude.

224 The relative suppression of the low energy gamma ray spectrum may be explained within a hadronic model for the  
 225 FBs wherein energy-dependent diffusion leads to a relative deficit of low energy protons at high latitudes. Specifically,  
 226 if protons are injected in the plane, the finite age of the FBs may only allow high energy protons to propagate to high  
 227 latitude thereby predicting a gradual hardening of the gamma ray spectrum with latitude.

228 In leptonic models the fast cooling of electrons means they cannot move too far from their accelerators and distributed  
 229 acceleration inside the FBs seems to be favored. For the case of stochastic acceleration the maximal electron energy  
 230 might be expected to be 1 TeV, implying the optical/UV and IR component of the ISRF may play an important role  
 231 in gamma ray production inside the FBs. However, the attenuation of these components of the ISRF at high latitudes  
 232 is, at least naively, in conflict with the observed hardening of the gamma ray spectrum in the highest slice of the South  
 233 Bubble unless a very specific electron spectrum evolution is realized.  
 234

## 235 References

- 236 Abdo et al. 2012, *Astrophys.J.Suppl.*, 199, 31  
 237 Ackermann, M., Ajello, M., Atwood, W. B., et al. 2012, *ApJ*, 750, 3  
 238 Ackermann, M. et al. 2012, *Astrophys.J.Suppl.*, 203, 4  
 239 Aharonian, F. A. & Atoyan, A. M. 1996, *A&A*, 309, 917  
 240 Bland-Hawthorn, J. & Cohen, M. 2003, *ApJ*, 582, 246  
 241 Bronfman, L., Casassus, S., May, J., & Nyman, L.-Å. 2000, *A&A*, 358, 521  
 242 Carretti, E., Crocker, R. M., Staveley-Smith, L., et al. 2013, *Nature*, 493, 66  
 243 Case, G. L. & Bhattacharya, D. 1998, *The Astrophysical Journal*, 504, 761  
 244 Cheng, K.-S., Chernyshov, D. O., Dogiel, V. A., Ko, C.-M., & Ip, W.-H. 2011, *ApJ*, 731, L17  
 245 Crocker, R. M. 2012, *MNRAS*, 423, 3512  
 246 Crocker, R. M. & Aharonian, F. 2011, *Physical Review Letters*, 106, 101102  
 247 Crocker, R. M., Bicknell, G. V., Carretti, E., Hill, A. S., & Sutherland, R. S. 2013, *ArXiv e-prints*  
 248 Dobler, G., Finkbeiner, D. P., Cholis, I., Slatyer, T., & Weiner, N. 2010, *ApJ*, 717, 825  
 249 Finkbeiner, D. P. 2004, *ApJ*, 614, 186  
 250 Gando Ryu, S., Nobukawa, M., Nakashima, S., et al. 2012, *ArXiv e-prints*  
 251 Guo, F. & Mathews, W. G. 2012, *ApJ*, 756, 181  
 252 Guo, F., Mathews, W. G., Dobler, G., & Oh, S. P. 2012, *ApJ*, 756, 182  
 253 Hooper, D. & Slatyer, T. R. 2013, *Physics of the Dark Universe*, 2, 118  
 254 Jones, D. I., Crocker, R. M., Reich, W., Ott, J., & Aharonian, F. A. 2012, *ApJ*, 747, L12  
 255 Lorimer, D. R., Faulkner, A. J., Lyne, A. G., et al. 2006, *MNRAS*, 372, 777  
 256 McQuinn, M. & Zaldarriaga, M. 2011, *MNRAS*, 414, 3577  
 257 Mertsch, P. & Sarkar, S. 2011, *Mem. Soc. Astron. Italiana*, 82, 876  
 258 Moskalenko, I. V. & Strong, A. W. 2000, *ApJ*, 528, 357  
 259 Planck Collaboration, Ade, P. A. R., Aghanim, N., et al. 2013, *A&A*, 554, A139  
 260 Snowden, S. L., Egger, R., Freyberg, M. J., et al. 1997, *ApJ*, 485, 125  
 261 Su, M. & Finkbeiner, D. P. 2012, *ApJ*, 753, 61  
 262 Su, M., Slatyer, T. R., & Finkbeiner, D. P. 2010, *ApJ*, 724, 1044



- 263 Vladimirov, A. E., Digel, S. W., Jóhannesson, G., et al. 2011, *Computer Physics Communications*, 182, 1156  
264 Yang, H.-Y. K., Ruszkowski, M., Ricker, P. M., Zweibel, E., & Lee, D. 2012, *ApJ*, 761, 185  
265 Yusifov, I. & Küçük, I. 2004, *A&A*, 422, 545  
266 Zubovas, K., King, A. R., & Nayakshin, S. 2011, *MNRAS*, 415, L21  
267 Zubovas, K. & Nayakshin, S. 2012, *MNRAS*, 424, 666